QNH: Design and Test of a Quasi-Nonhydrostatic Model for Mesoscale Weather Prediction

A. E. MACDONALD

NOAA/ERL/Forecast Systems Laboratory, Boulder, Colorado

J. L. LEE

NOAA/ERL/Forecast Systems Laboratory, Boulder, Colorado, and CIRA, Colorado State University, Foothills Campus, Fort Collins, Colorado

S. SUN

NASA Goddard Institute, New York, New York

(Manuscript received 8 June 1998, in final form 19 March 1999)

ABSTRACT

A new mesoscale weather prediction model, called QNH, is described. It is characterized by a parameter that multiplies the hydrostatic terms in the vertical equation of motion. Models of this type are referred to generically as ''quasi-nonhydrostatic.'' The quasi-nonhydrostatic parameter gives the model a character that is essentially nonhydrostatic, but with properties that are theoretically thought to result in smoother, more accurate, and stable predictions. The model is unique in a number of other aspects, such as its treatment of lateral boundary conditions, the use of explicit calculation in the vertical direction, and the use of the bounded derivative theory for initialization. This paper reports on the design and test of the QNH model, which represents the first time the applicability of this type of model has been demonstrated for full-physics, mesoscale weather prediction. The dynamic formulation, discretization, numerical formulation, and physics packages of the model are described. The results of a comprehensive validation of the model are presented. The validation includes barotropic, baroclinic (Eady wave), mountain wave, tropical storm, and sea breeze tests. A simulation of a winter storm (with updated lateral boundary conditions) is presented, which shows that the model has significant skill in forecasting terrain-forced heavy precipitation. It is concluded that the QNH model may be valuable for mesoscale weather prediction.

1. Introduction

A new and unique mesoscale weather prediction model, named QNH (for quasi-nonhydrostatic), has been developed at the National Oceanic and Atmospheric Administration's Forecast Systems Laboratory. A description of the model and the results of a test program are presented in this paper. The model is characterized by a parameter that multiplies the hydrostatic term in the vertical equation of motion. We refer to this class of models generically as ''quasi-nonhydrostatic.'' They are based on a theory of fluid models originally outlined by Kreiss (1980), and first scaled and adapted for weather prediction by Browning and Kreiss (1986).

A companion paper, MacDonald et al. (2000), discusses the application of the theory to the mesoscale weather prediction problem. A third paper, Lee and MacDonald (2000), scales, derives, and demonstrates the use of the bounded derivative initialization in the QNH model. This work is the first application of the Browning and Kreiss (1986) theory in a full physics, mesoscale weather prediction model, and thus addresses the question of the practical importance of the theory. The applicability of important ideas such as making the hyperbolic prediction equations more symmetric (which should result in more stable and accurate numerical integrations), bounded derivative initialization, well-posed lateral and top boundaries, and explicit calculation along the vertical coordinate are all tested, and discussed in the paper.

The paper presents the design of the QNH model and summarizes a test program that was conducted to determine the validity of the model. Since the model is based on new concepts, and is quite different from existing hydrostatic or nonhydrostatic models, the main goal of the paper is to establish the credibility of this

Corresponding author address: Dr. A. E. MacDonald, NOAA/ERL, R/E/FS, 325 Broadway, Boulder, CO 80523.

Unauthenticated | Downloaded 10/04/22 02:19 PM UTC

new approach to weather prediction. Its actual value cannot be established by a limited test program—it must be used in prediction for a period of time adequate to quantitatively compare its predictions with other forecast models. In the conclusion, plans for such a test are briefly discussed.

A defining attribute of quasi-nonhydrostatic models is the quasi-nonhydrostatic parameter, referred to in this paper as "α." This is a parameter that multiplies the hydrostatic balance terms of the vertical equation of motion. In a QNH model it is chosen as a fraction of 1. As discussed in MacDonald et al. (2000), it is typically set to the square of the aspect (height–width) ratio of the meteorological phenomena of interest. It is desirable to make the vertical and horizontal grid spacing such that:

$$\alpha = \left(\frac{\Delta z}{\Delta x}\right)^2.$$

When α is equal to 1, the model is purely nonhydrostatic. When it is less than 1, it slows the propagation speeds of the high-frequency inertia gravity and acoustic modes, while having no effect on the speed of the meteorologically significant low-frequency rotational (Rossby) modes. A linear analysis in MacDonald et al. (2000) shows that it acts as a bandpass filter, decreasing the speed and amplitude of the high-frequency gravity waves, while leaving the lower-frequency gravity waves unmodified. When the value of α is smaller than unity, it decreases the speed at which a model can reach hydrostatic equilibrium. Thus, as discussed in Browning and Kreiss (1986), care must be taken to not let significant energy in high-frequency modes into the integration. Typically this is done by initialization, and by filtering forcing terms such as diabatic heating to assure they are smooth.

The main objective of the QNH model is to make accurate forecasts of mesobeta-scale and larger phenomena, particularly clouds and precipitation. The mesobeta classification, originated by Orlanski (1975), includes horizontal phenomena with wavelengths between 20 km and 200 km. If the vertical scale height of the atmosphere is taken as 10 km, then the 100-km-scale length would have a quasi-nonhydrostatic parameter of 10^{-2}:

$$\alpha = \left(\frac{10}{100}\right)^2 = 10^{-2}.$$

In MacDonald et al. (2000) a notation for referring to quasi-nonhydrostatic models is presented. The order of magnitude of the negative exponent of α is appended to the model name to indicate its type. Thus, a mesobeta model with an exponent of -2, as discussed above, would be a QNH2 model. A mesoalpha-scale model would be a QNH3, and a fully nonhydrostatic model would be a QNH0.

As discussed in MacDonald et al. (2000), QNH2 should be accurate for Rossby waves, forced circulations such as those created by latent heating, and larger-scale gravity waves. Small scale, high-frequency gravity wave responses to impulses are decreased in frequency and amplitude. Small-scale, vertically propagating mountain waves can be improperly ducted, as pointed out by Skamarock and Klemp (1994). This deficiency was analyzed, and corrective techniques were identified in MacDonald et al. (2000). For example, the terrain used in the model can be truncated, eliminating the Fourier components of scales smaller than those that the model handles appropriately. The QNH model has been tested with horizontal grid mesh lengths between 5 km and 20 km, and will be shown to give realistic results for phenomena like tropical storms and midlatitude heavy precipitation.

Design goals of the QNH model included simplicity and accuracy. The inherent simplicity of the model is made possible by some of the unique attributes of quasi-nonhydrostatic models. The use of explicit calculation for vertical quantities makes the vertical coordinate similar to the horizontal coordinate in the finite-difference formulation. As discussed in section 2b, fourth-order time and space finite differencing was used in the vertical and horizontal, which resulted in highly accurate computations. A disadvantage of quasi-nonhydrostatic models is that once the horizontal grid length and quasi-nonhydrostatic parameter are chosen, the optimum vertical grid length is determined, as shown in section 2b.

The simplicity of the model allowed us to make the computer implementation quite efficient. The model equations themselves have a small number of terms, and are formulated in a terrain-following coordinate system. This allowed us to parallelize it in the horizontal, and to vectorize on the vertical coordinate. Techniques were used to make the model optimized for both single processor calculations (e.g., coding for cache coherence and unbroken pipelining) and multiple processor applications (e.g., minimizing latency associated with halo exchanges; Baillie et al. 1995, 1996). Thus while the model uses a short time step (8 s for a 20-km horizontal grid mesh) it runs efficiently and rapidly on a parallel computer. For example, a parallel benchmark of QNH and the hydrostatic Mesoscale Analysis and Prediction System (MAPS; Bleck and Benjamin 1993) model shows that the two models have about the same run time, even though the time step for MAPS is 30 s—much longer than QNH.

In the conclusion we discuss how QNH has satisfied criteria for acceptance of a new model, and the potential future role of the model.

2. Design and description

The QNH model is quasi-nonhydrostatic, fully compressible, and Eulerian. Table 1 summarizes its main characteristics, and lists some of the options tested. The first bullet under each option is the primary; for example, fourth-order space differencing was used almost

Unauthenticated | Downloaded 10/04/22 02:19 PM UTC

TABLE 1. QNH options and reference.

Category	Options	References and remarks
Dynamic equations	*Quasi-nonhydrostatic, compressible $0 < \alpha \leq 1$	Browning and Kreiss (1986)
Vertical coordinate	*Terrain following sigma z (Cartesian)	Browning and MacDonald (1993) Gal-Chen and Somerville (1975)
Vertical dynamics	*Explicit	Browning and Kreiss (1986)
Horizontal coordinate	*Cartesian Lambert	Haltiner and Williams (1980)
Grid stagger	*Arakawa C Grid (3D)	Arakawa and Lamb (1977)
Time differencing	*3d-order Adams–Bashforth	Durran (1991), 4th Order accuracy
	*3d-order Adams Moulton	Gustafsson et al. (1995)
Space differencing	*4th order	Haltiner and Williams (1980)
	*2d order	
Lateral boundary	*Well-posed	Oliger and Sundstrom (1978)
Upper boundary	*Well-posed	Oliger and Sundstrom (1978)
Lower boundary	*Kinematic	Haltiner and Williams (1980)
Initialization	*Bounded derivative	Lee and MacDonald (2000)
Microphysics	*Schultz	Schultz (1995)
	*MM5	Grell et al. (1994)
	*ARPS	Tao and Simpson (1993)
Cumulus	*Kuo	Kuo (1974)
Turbulence	*Mellor–Yamada 2.0	Mellor and Yamada (1974)
	*Drag	
Diffusion	*4th order	Haltiner and Williams (1980)
	*2d order	
Radiation	*MacDonald	Pielke (1984)
Surface forcing	*Slab	Pielke (1984)

exclusively, and the Schultz microphysics was used for most of the tests. In this section each of the main packages that were used in the model are briefly described.

a. Dynamics and topography

The basic dynamic equations are formulated similar to Browning and Kreiss (1986) with the exception that perturbation potential temperature, rather than its inverse, is used:

$$\frac{du}{dt} = -\frac{1}{\rho_0}\frac{\partial p}{\partial x} + fv \tag{1}$$

$$\frac{dv}{dt} = -\frac{1}{\rho_0}\frac{\partial p}{\partial y} - fu \tag{2}$$

$$\frac{dw}{dt} = \alpha\left[-\frac{1}{\rho_0}\frac{\partial p}{\partial z} + g\theta - \frac{g}{\gamma P_0}p\right] \tag{3}$$

$$\frac{dp}{dt} = -\gamma P_0\left(\frac{\partial u}{\partial x} + \frac{\partial v}{\partial y} + \frac{\partial w}{\partial z}\right) + \rho_0 g w \tag{4}$$

$$\frac{d\theta}{dt} = -\tilde{\theta}w, \tag{5}$$

where u, v, and w are the x, y, and z components of wind velocity, p is the perturbation pressure, θ is the perturbation potential temperature defined by

$$\theta = \frac{\theta_{\text{total}}}{\overline{\theta}(z)} - 1,$$

where θ_{total} = potential temperature. The constants γP_0 and $\tilde{\theta}$ are given by

$$\gamma P_0 = 1.4 \times 10^5 \qquad \tilde{\theta} = \frac{1}{\overline{\theta}(z)}\frac{\partial \overline{\theta}}{\partial z}.$$

The total derivative is given by

$$\frac{d}{dt} = \frac{\partial}{\partial t} + u\frac{\partial}{\partial x} + v\frac{\partial}{\partial y} + w\frac{\partial}{\partial z}.$$

In the above presentation of the basic equations the metric and forcing terms were omitted for simplicity; the forcing terms are introduced later.

This set of five prognostic equations with five unknowns is derived from the conservation relations for momentum, mass, and thermodynamic energy. Density has been eliminated from the prognostic set by use of the equation of state, and appears in the prognostic set as ρ_0, a function of z, which is constant in time.

This system must be transformed for use over topography. The complete set of dynamic equations used in the QNH model are derived from the basic dynamic equations in a manner similar to Browning and MacDonald (1993). After coordinate transformation of the independent and dependent variables the quasi-nonhydrostatic system becomes:

$$\frac{du'}{dt'} = -\frac{1}{\rho_0}(p_{x'} - z_{x'}z'_z p_{z'}) + fv'$$

$$\frac{dv'}{dt'} = -\frac{1}{\rho_0}(p_{y'} - z_{y'}z'_z p_{z'}) - fu'$$

Unauthenticated | Downloaded 10/04/22 02:19 PM UTC

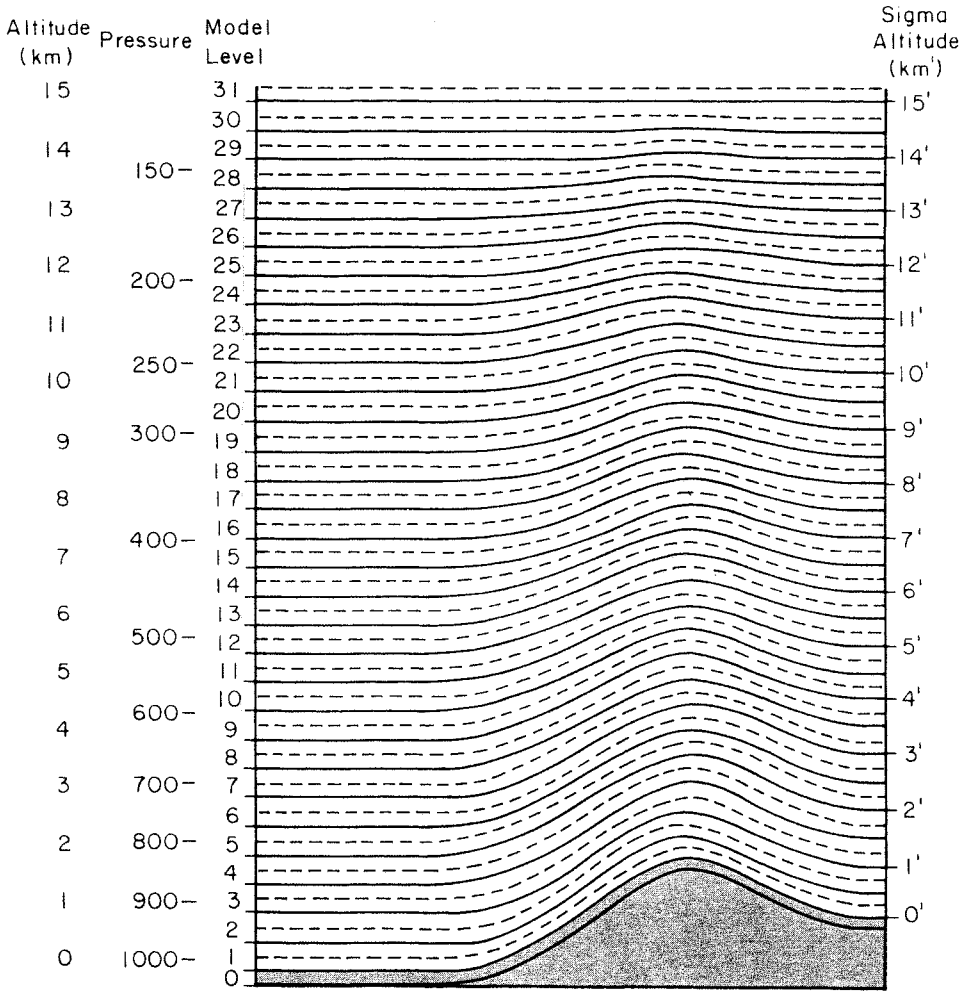

FIG. 1. An example of the vertical coordinate system. Each layer is 500 m thick, with a dashed line in the middle. The solid lines are where the vertical velocity is defined. Note that the first level of the main variables is at 250 m, the second is at 750 m, etc. Level 1 for the vertical velocity is at 500 m, while level 0 is at the surface. The actual altitude in kilometers is shown on the left, while the terrain transformed coordinate altitude is shown on the right with primes. The shaded area on the bottom represents terrain.

$$\frac{dw}{dt'} = -\alpha\left[\frac{1}{\rho_0}z'_z p_{z'} + \left(\frac{g}{\gamma P_0}\right) - g\theta'\right]$$

$$\frac{dp}{dt} = -\gamma P_0[(u'_{x'} + v'_{y'} + z'_z w_{z'}) - z_{x'}z'_z u'_{z'} - z_{y'}z'_z v'_{z'}] + \rho_0 g w$$

$$\frac{d\theta}{dt} = -\tilde{\theta}w + \frac{h}{C_p T}.$$

where h is the heating rate, T is the temperature, and C_p is the specific heat at constant pressure. The primes indicate the transformed variables.

The vertical velocity in the transformed coordinate system is

$$w' = z'_z(w - z_{x'}u' - z_{y'}v').$$

The QNH model uses a terrain-following sigma z vertical coordinate (Gal-Chen and Somerville 1975) given by

$$z' = zt \cdot (z - zb)/(zt - zb),$$

where

zb = altitude of the terrain,

zt = height of model top.

Figure 1 gives an example of the vertical Cartesian coordinate system. The vertical mesh length is 500 m, and the vertical velocity is defined at intermediate levels as discussed below. In this case, the vertical mesh length of 500 m could be used with different types of QNH models, as discussed below.

b. Discretization in space

The QNH model uses the C grid (Arakawa and Lamb 1977), in the vertical as well as the more customary

Unauthenticated | Downloaded 10/04/22 02:19 PM UTC

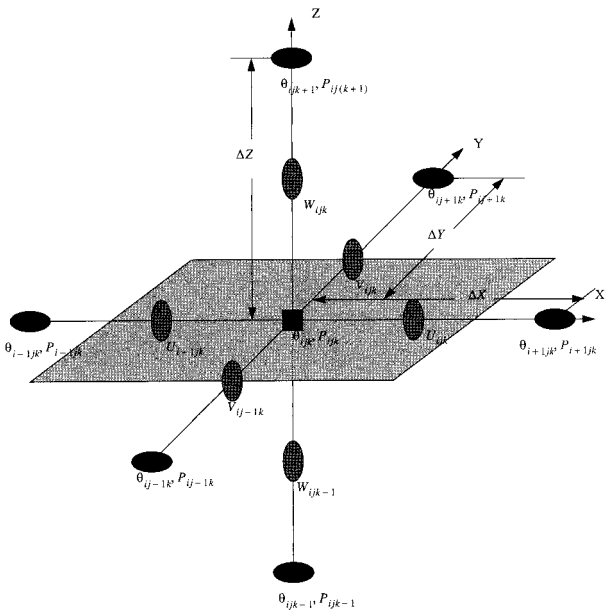

FIG. 2. Schematic of the dependant variables and their location on the C grid. The perturbation potential temperature and perturbation pressure are located at the center point, designated as a rectangle. The momentum variable, *u*, *v*, and *w*, are staggered one-half grid point in the positive direction, and designated as vertical ovals. The perturbation potential temperature and pressure of the neighboring grid points are shown as horizontal ovals.

horizontal implementation. In other words, the momentum variable, w, is staggered vertically in the same way as the momentum variables of the C grid are scattered in the horizontal. Figure 2 shows how the primary variables appear on the grid. The momentum variables, *u*, *v*, and *w* are staggered half a grid mesh distance in the positive direction. The other two dynamic variables, *p* and θ, as well as other scalar variables such as water vapor specific humidity, are defined at standard points on the main grid. In this discussion we refer to ''momentum points'' and ''standard points.'' The C grid gives high accuracy in the calculation of divergence (Haltiner and Williams 1980). Although both second and fourth-order space differencing were implemented for QNH, the fourth-order scheme was predominantly used.

When discretizing in the vertical for use in explicit calculation of the vertical equations, consideration must be given to the horizontal and vertical scales of interest. Although it is not required, modelers will often want to use spatial grid mesh distances such that the time step is the same for the vertical and horizontal directions. These are related through the quasi-nonhydrostatic parameter, $\alpha = (\Delta z/\Delta x)^2$. Two examples of how this affects the design of the model are presented. First, consider a model that is intended to resolve the ''middle'' of the mesobeta scale, that is, waves of $L = 4\Delta x = 80$ km size, and larger. Further, suppose that 500-m resolution in the vertical is deemed adequate to resolve the phenomena of interest (e.g., Rossby, gravity, and forced waves). Then $\alpha = (0.5/20)^2 = 0.000\,625$. As discussed in section 1, this is classified as a QNH3 model, although it is at the high end of the range. In a second example, suppose that the entire mesobeta range is to be resolved. Then we might use $\Delta x = 5$ km, $\Delta z = 500$ m, and $\alpha = 0.01$, giving a QNH2 model, which resolves $4\Delta x = 20$ km waves. Since the vertical resolution and coordinate system of the two models are the same, $\Delta z = 500$ m, it would be straightforward to nest a QNH2 model with higher resolution ($\Delta x = 5$ km) inside a QNH3 model of lower resolution ($\Delta x = 20$ km). The nesting could be done dynamically such that the higher resolution nest was called only when smaller-scale phenomena appeared in the model integration.

A goal of the QNH model effort was good prediction of cloud and precipitation. We believe that a QNH2 model with horizontal resolution of 10 km, vertical resolution of 1 km, and $\alpha = 0.01$ would capture most of the significant precipitation causing waves. This is partly based on scaling considerations that indicate that significant precipitation requires significant vertical extent in the troposphere. Resolution of 1000 m in the lower layers, however, would be quite poor for the boundary layer. A solution could be to ''nest'' in the vertical, with a QNH4 model in the lower kilometer or two, with horizontal resolution of 10 km (same as the model above), and $\Delta z = 100$ m. The QNH4 model, with $\alpha = 0.0001$, would be appropriate for the small aspect ratio typical of boundary layer phenomena.

c. Time differencing

The primary time-differencing scheme used in the QNH model is the third-order Adams–Bashforth. The formula for this scheme is

$$u^{(n+1)} = u^{(n)} + \frac{\Delta t}{12}[23F^{(n)} - 16F^{(n-1)} + 5F^{(n-2)}],$$

where F is the ''tendency function.'' It is an explicit technique that requires just one forcing function evaluation per time step. It is important to note that is has fourth-order accuracy. It was chosen based on the analysis of Durran (1991), which showed that both the amplitude and phase errors are $O[(\Delta t)^4]$. It is not subject to time splitting instability, and is more accurate than the leapfrog scheme. An advantage of the scheme is that it requires no time filtering. A disadvantage is the need to maintain the forcing functions for three time levels in memory. It is reasonable to use a more memory intensive scheme like Adams–Bashforth because the relative cost of memory is small compared to the savings in reducing the number of calculations. The model uses forward differencing for the first time step (equivalent to first-order Adams–Bashforth), second-order Adams–Bashforth for the second time step, and third-order Adams–Bashforth for the remaining time steps. Based on an analysis in Gustaffson et al. (1995), the third-order

Unauthenticated | Downloaded 10/04/22 02:19 PM UTC

Adams–Moulton scheme was tested. It was thought that efficiency could be increased because of the potential for a much longer time step. A predictor–corrector mode was implemented:

$$u^{(n+1)} = u^{(n)} + \frac{\Delta t}{24}[9F^{(n+1)} + 19F^{(n)} - 5F^{(n-1)} + F^{(n-2)}].$$

Although this scheme was easily created by a modification of the third-order Adams–Bashforth code, it did not turn out to be efficient. The Adams–Moulton scheme typically required multiple iterations to converge (i.e., to keep the integration stable), which increased the number of calculations needed per unit of model prediction beyond that needed for the third-order Adams–Bashforth. This result accords with the analysis of Durran (1991) with regard to the relative efficiency of Adams–Bashforth and Adams–Moulton.

Analyzing the Adams–Bashforth scheme for stability gives the following formula for a three-dimensional model:

$$\omega^*\Delta t < \frac{0.724}{(3)^{1/2}},$$

where

$$\omega^* = \frac{2C \sin\left(\frac{k\Delta x}{2}\right)}{\Delta x}.$$

The calculated time step of QNH for a 20-km model using this formula would be 14 s. However, in the winter storm case we used an 8-s time step.

d. Initial and boundary conditions

The initialization for the QNH model using the bounded derivative principle is detailed in a companion paper, Lee and MacDonald (2000). The theory of the bounded derivative allows the initialization to constrain the time derivatives to any order; as used in the QNH initialization, constraining the time derivatives to the second order proved generally adequate. It was found that the bounded derivative initialization worked well, even when challenged by the complex terrain of western United States, which was the setting for the winter storm test. It also can accommodate forcing fields such as those caused by latent heating, into the initialization. The bounded derivative initialization entails solving two three-dimensional elliptic equations, one that relates the three-dimensional pressure field to the velocity fields (similar to the nonlinear balance equation), and a second that relates the vertical velocity to the divergent horizontal velocity. The computational load is equivalent to that of making a several hour model prediction. The vertical velocity equation is solved using a kinematic condition of vanishing vertical velocity on the bottom, and a mixed (Dirichlet and Neumann) condition on the top. The pressure equation is solved with Neumann boundary conditions on the sides, and mixed on the top and bottom. The initialization is not sensitive to friction; it starts smoothly whether or not it is included. During the integration we used a free slip lower boundary.

It is generally convenient to not use the lateral boundary condition from the larger-scale model at every time step, but rather to pick an interval, and to interpolate in time for the value of the variables on the boundary. This raises the question of how often the larger (or outer) model boundary values should be used. The question is not academic, because as discussed above, each actual (i.e., not interpolated in time) usage of the boundary conditions from the outer model requires solution of the bounded derivative over the whole domain of the limited-area model. Physically, if phenomena (e.g., Rossby waves) are going to propagate from the outer model into the limited domain, the boundary time resolution must be adequate to resolve such waves. An experiment was conducted to test the time resolution needed for a small wave to enter the prediction domain without excessive error. Circular waves of various dimension were allowed to propagate from the western boundary into the domain. It was found that, for mesoscale circulations, and reasonable values of flow, a 6-h time interpolation was adequate. For a margin of safety, we have routinely used 3-h fields from the outer models.

In MacDonald et al. (2000) it describes how a well-posed boundary allows waves to propagate through, and not reflect back into a model domain. In QNH these boundary conditions were used on the lateral and upper boundaries. Although we experimented with the use of a sponge for the upper boundary, it was determined that reflection and accumulation of energy near the top was not a problem—the well-posed open upper boundary was sufficient. The ability to allow acoustic and gravity waves to propagate smoothly through the boundaries, rather than spuriously reflect, is a valuable characteristic for a limited-area model. In the real atmosphere, dispersive waves that propagate in two or three dimensions will result in a decrease of wave energy in a given limited domain because they eventually leave through the boundary. A model that spuriously reflects these back into the inner domain could have difficulties due to the false wave energy and its growth and interaction through time.

e. Microphysics and cumulus paramaterization

The QNH model has a full microphysical paramaterization, consisting of six moisture specific content (q, in units of kilograms per cubic meter) variables:

qv: water vapor
qw: cloud water
qi: cloud ice
qr: rain
qs: snow
qg: graupel.

Unauthenticated | Downloaded 10/04/22 02:19 PM UTC

The primary microphysics package was based on Schultz (1995). It was recoded and adapted slightly for use in QNH. The Shultz microphysics package is designed for speed and simplicity, with most phase conversions being related by simple linear expressions, using adjustable constants of proportionality. As computers become faster and models reach higher resolution in time and space, the accuracy of such linear approximations should become better. QNH was also tested with two other microphysical packages, one from the Mesoscale Model 5 model (Grell et al. 1994; Dudhia 1993), and another from the Advanced Regional Prediction System (ARPS) model (Tao and Simpson 1993). These gave predictions similar to the Schultz package, but required up to 25% longer computing time in the winter storm case. The availability of the different microphysical packages will allow determination of whether the faster Schultz package is useful in other weather situations, such as warm season rain. The Kuo (1974) cumulus paramaterization was implemented for the QNH model. Its effect in the winter storm case was relatively minor; it is further discussed in sec 3f. To maintain the moisture variables as positive, a forward upstream moisture advection scheme is used in QNH. The moisture advection scheme has only first-order accuracy in space, unlike the rest of the space differencing, which has fourth-order accuracy.

f. Turbulence and diffusion

Two turbulence packages have been implemented for the QNH model. The first is the well-known Mellor–Yamada (1974) 2.0 closure scheme, and the second is a simple drag model, which will be briefly discussed. The Mellor–Yamada 2.0 does not advect turbulent energy, but seemed to give reasonable results in the sea breeze and tropical storm simulations. However, the resolution in the boundary layer of only 500 m is poor compared to the phenomena of interest, and compared with other models. One solution to this problem would be to vertically nest a higher resolution boundary layer with an internal well-posed boundary as discussed in sec 2b. However, a common practice is to have variable vertical resolution, with higher resolution near the surface, to adequately resolve boundary layer effects. This approach would require a variable quasi-nonhydrostatic parameter if it were to be implemented in QNH. It was briefly investigated, appears to be feasible, and is a subject for future efforts. A third approach is possible in which a simple boundary layer model (not a full dynamic model) is coupled to the main model using forcing. This simple approach will probably be the first to be tried.

A simple drag formulation of the effect of low-level turbulence was implemented in QNH. In this approach, the effects of surface-based momentum fluxes are to retard the wind velocity by arbitrary but reasonable amounts in the lower layers. The results of this simple approach was a reasonable low-level flow field for the winter storm simulation.

Two types of diffusion were implemented in QNH (Haltiner and Williams 1980). The first was a standard second-order formula, and the second was a fourth-order scheme:

$$\text{second-order diffusion in } x = \mu_x \frac{\partial^2 F}{\partial x^2},$$

$$\text{second-order diffusion in } z = \mu_z \frac{\partial^2 F}{\partial z^2},$$

$$\text{fourth-order diffusion in } x = -\mu_x \frac{\partial^4 F}{\partial x^4},$$

$$\text{fourth-order diffusion in } z = -\mu_z \frac{\partial^4 F}{\partial z^4},$$

where

$$\mu_x = \frac{5.0 \times 10^{-4}}{(\Delta x)^4}, \qquad \mu_z = \frac{5.0 \times 10^{-4}}{(\Delta z)^4}.$$

In the current version of the model the cross terms were omitted based on scaling considerations.

g. Radiation and surface forcing

The design of QNH required a radiation package that included one-dimensional radiation effects, and was simple and computationally efficient. To meet this goal, a radiation paramaterization, which has both shortwave and longwave bands, was developed for QNH by MacDonald. The package draws mainly from the radiation discussion by Pielke (1984), but also includes elements from Haltiner and Williams (1980) and Washington and Parkinson, (1986). The shortwave radiation is calculated for two bands, visible (0.2–0.75 μm) and near infrared (0.75–4 μm). It calculates the heating of the atmosphere at all three-dimensional grid points, and also calculates the shortwave heating at the surface and the shortwave outgoing radiation at the top of the atmosphere. The package divides the total solar radiation of 1367 W m^{-2} incident at the top of the atmosphere, giving 55% to the visible, and 45% to the near infrared. The effects of the shortwave radiation are calculated by allowing a downward transit of the atmosphere, and calculating a reflection, transmission and heating budget. Shortwave radiation, which reaches the surface, is divided using the albedo between that which is passed on to the surface package as heating, and that which is reflected back upward into the atmosphere. The treatment for upward shortwave is similar to that described above for downward shortwave. The microphysics package is used to identify cloudy layers, and the paramaterization of Stephens (1978) is used in clouds. Stephen's treatment of the shortwave transmission in cloudy air was the primary reason for separating the shortwave into two bands. MacDonald simplified the longwave radiation

Unauthenticated | Downloaded 10/04/22 02:19 PM UTC

calculation by starting at the surface, allowing longwave radiation to transmit up, and be modified by the emissivity in clear and cloudy air layers. Then a similar calculation is done for each of the cloud layers obtained from the microphysics package. Pielke's (1984) formula 8-41 was used for the flux divergence in clear air, and Stephen's (1978) treatment was used in the cloudy air. The output of the longwave heating routine includes longwave heating as a function of three dimensions in units of watts per kilogram longwave heating at the surface, and longwave outgoing radiation at the top of the atmosphere.

A simple package was developed for surface interaction in QNH. The surface is idealized as a slab of variable thickness, depending on the surface substance. The bottom of the slab is held at constant temperature, which corresponds to the depth at which diurnal temperature changes are small. The temperature is taken as (typically) a monthly average of surface temperature. Different surface types (e.g., water, clay, ice, etc.) are represented, with values of specific heat and density from Pielke's (1984, Table 11-3). A bucket model of soil moisture was also included. The result is a constant that relates the heat forcing from shortwave and longwave radiation and evaporation, to the change of temperature of the surface slab. A drag formula (in which the heat flux is proportional to temperature difference and wind velocity) is used to exchange heat between the surface and the lower three layers of the model.

h. Heat and momentum coupling

As a result of water phase change, turbulence, radiation, and surface effects, the dynamic portion of the model must accommodate the associated heat and momentum forcing. In this discussion the coupling of the heat and momentum into the dynamic portion of the model is summarized. The thermodynamic equation in the dynamics portion of the model has the form:

$$\frac{d\theta}{dt} = -\tilde{\theta}w + \frac{1}{C_pT}(\mathrm{HM} + \mathrm{HR} + \mathrm{HT} + \mathrm{HS}),$$

where

HM = heating due to moisture phase change,
HR = heating due to radiation,
HT = heating due to turbulent flux,
HS = heating due to surface forcing.

Turbulent momentum fluxes enter the dynamic equations in the horizontal momentum equations:

$$\mathrm{turb}x = \frac{1}{\rho_0}\frac{\partial \tau_u}{\partial z} \qquad \mathrm{turb}y = \frac{1}{\rho_0}\frac{\partial \tau_v}{\partial z},$$

where diffusion and terrain effects have been omitted for clarity.

An important aspect of quasi-nonhydrostatic models is that the forcing should be ''smooth'' as it affects the dynamic portion of the model. In the case of QNH, the smoothness in time and space can be assured as the forcing terms, HM, HR, HT, HS, turb*x*, and turb*y* are injected into the dynamic calculations. Specifically, the forcing terms can be smoothed over space (e.g., using a Fourier transform and dropping higher wavenumbers) after the physics calculation and before they are used in the dynamics. In the initial test phase spatial smoothing proved unnecessary; however, the model has been structured to allow easy implementation of this feature.

There are two reasons for coupling forcing into the dynamic model smoothly in time. First, as discussed in MacDonald et al. (2000), the theory of quasi-nonhydrostatic models requires smoothness in the forcing terms. Second, since the time step for the dynamic part of mesoscale models is so short, the calculation of the microphysics and other forcing less often than every time step makes the model more efficient. Experience with the 20-km version of QNH showed that calculating the physics every 100 time steps, about every 800 s, with a smooth interpolation for the intermediate times, was optimal. When the microphysics forced heating was injected every time step, it generated instability due to forcing roughness, as suggested by the Browning and Kreiss (1994) theory.

3. Test program

A full-physics weather prediction model is very complex, and requires a comprehensive test program to exercise and validate all of its elements. Approximately a dozen types of tests of QNH were run, each with an extensive set of runs with varying parameters, length scales, initial conditions, etc. The six most important tests, and the elements of the model that they exercise are summarized in Table 2. As shown in the table, every major model element was specifically tested at least two times in the test program. The solid circle indicates the primary test, in which an element was carefully scrutinized to assure it was working properly in the model. The open circles indicate a test in which the element was also specifically examined. Each of the six tests is described and discussed in this section.

a. Barotropic steady-state vortex

The first and simplest test for the QNH model was to define a mesoscale, steady-state vortex, and to see if the model maintained the vortex properly. The steady state is defined such that the inertial and advective terms for all quantities are in balance, similar to Browning and Kreiss (1994). In the case described, the vertical velocity is initialized to 0 over the entire domain, but allowed to vary with time.

Although many runs were made with different scales, the results of the smallest scale test are discussed first, because it has the most significance for mesobeta-scale prediction. Two tests at this scale were run. In both cases

Unauthenticated | Downloaded 10/04/22 02:19 PM UTC

TABLE 2. A summary of the tests done to validate the QNH model. The solid circle indicates the primary test for a model element; the open circle indicates additional tests.

Summary of test program						
	Test program					
Model element	Barotropic vortex	Baroclinic wave	Mountain wave	Tropical storm	Sea breeze	Winter storm
Dynamics	○	●	○			
Advection	●	○	○			
Diffusion	○	●		○		
Initialization				○		●
Lateral boundaries				○	○	●
Space differencing	●	○				○
Time differencing	●	○				○
Topography			●			○
Microphysics				○	○	●
Cumulus						●
Radiation				○	●	○
Surface forcing				○	○	●
Turbulence				●	○	○

the domain of the model was 640 km, and the *e*-folding radius of the vortex was 60 km. The first run used a quasi-nonhydrostatic parameter of $\alpha = 10^{-2}$ (i.e., a QNH2 model), with a horizontal resolution of 20 km, and a vertical resolution of 1 km. The time step on the first run was 10 s. The second run was at half the horizontal resolution, 10 km, and half the vertical resolution, 500 m. The result of the test was that the vortex maintained a steady state, and the truncation error grew at a rate approximately 16 times as fast on the coarse mesh as the fine mesh, which is what is expected for fourth-order differencing. A second, similar test was run at larger scales, with a horizontal domain of 3200 km $\times$ 3200 km, a horizontal grid mesh of 100 km (first test) and of 50 km (second test). The vertical resolution on the coarse mesh was 1 km, and on the fine mesh, 500 m. The results of the large-scale test are shown in Fig 3. The growth of errors for the two runs are plotted, with line A representing the coarse mesh run error, line B representing the fine mesh run, and line C representing 16 times the error of the fine mesh run. Notice that the coarse mesh error closely approximates 16 times the fine mesh error, as it should for fourth-order space differencing. The other fields, pressure, temperature, and the northerly component of the wind behaved similarly. The vertical velocity stayed very small, as expected.

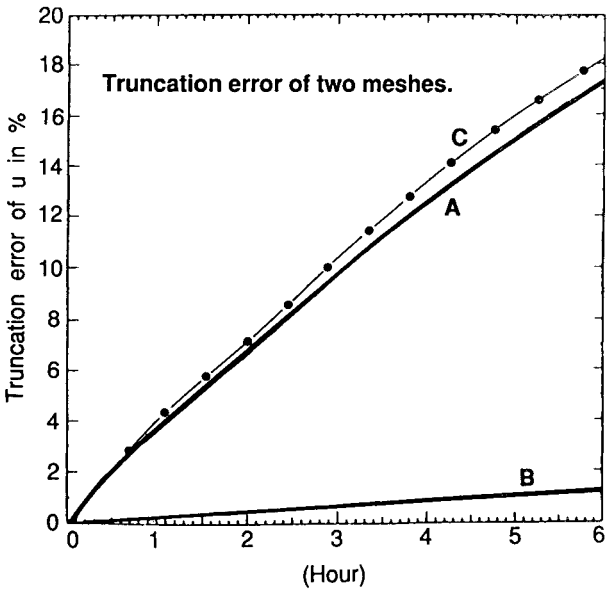

FIG. 3. A plot of the truncation error of the two model runs compared with the analytic solution. Line A is the coarse mesh truncation error, line B is the fine mesh truncation error, and line C is 16 times the fine mesh error. Notice that the coarse mesh error approximates 16 times the fine mesh error, as it should for fourth-order differencing.

b. Baroclinic (Eady) waves

Baroclinic waves play an important role in understanding energy conversions and frontogenesis. Many simplified theoretical models have been developed, which have analytic solutions that describe the unstable growth of the baroclinic waves. In recent years, these analytical models have become useful verification tools for a full nonlinear model (Snyder et al. 1991) under development. In this study, the semigeostrophic (S–G) analytic solution derived from an analytical model (Hoskins 1976) is used to compare with the growth of baroclinic waves in the QNH model. The S–G solution was derived from the hydrostatic and anelastic equations, with the geostrophic momentum approximation.

To simplify the problem, Hoskins (1976) derived the S–G analytic solution on a basic state of zonal flow with a constant vertical shear and no latitudinal shear. With the use of geostrophic coordinates and neglecting small terms, he was able to derive the following governing equations, which are identical to those solved in the classical Eady wave problem:

Unauthenticated | Downloaded 10/04/22 02:19 PM UTC

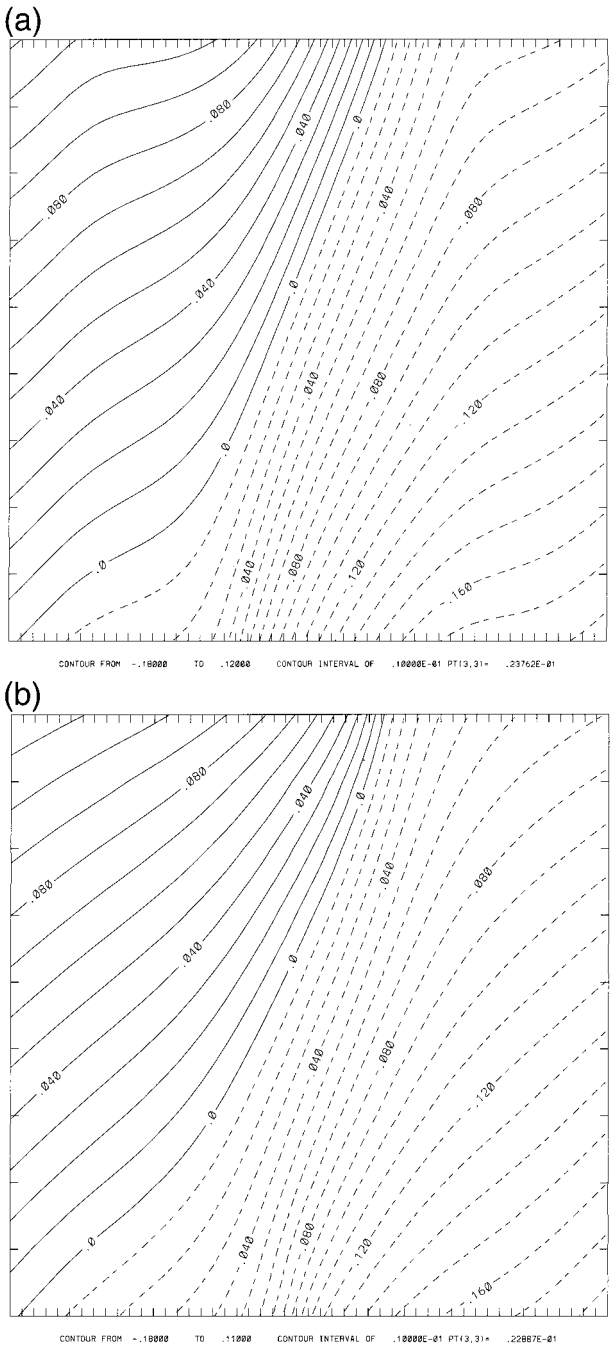

FIG. 4. Eady (baroclinic) wave study. Vertical crossection of (non-dimensional) perturbation potential temperature, θ, from the (a) S–G analytic solution, and from the (b) QNH model. The time is 120 h into the prediction, the vertical domain is 9 km, and the horizontal domain is 5000 km × 5000 km. South is on the left in the figures.

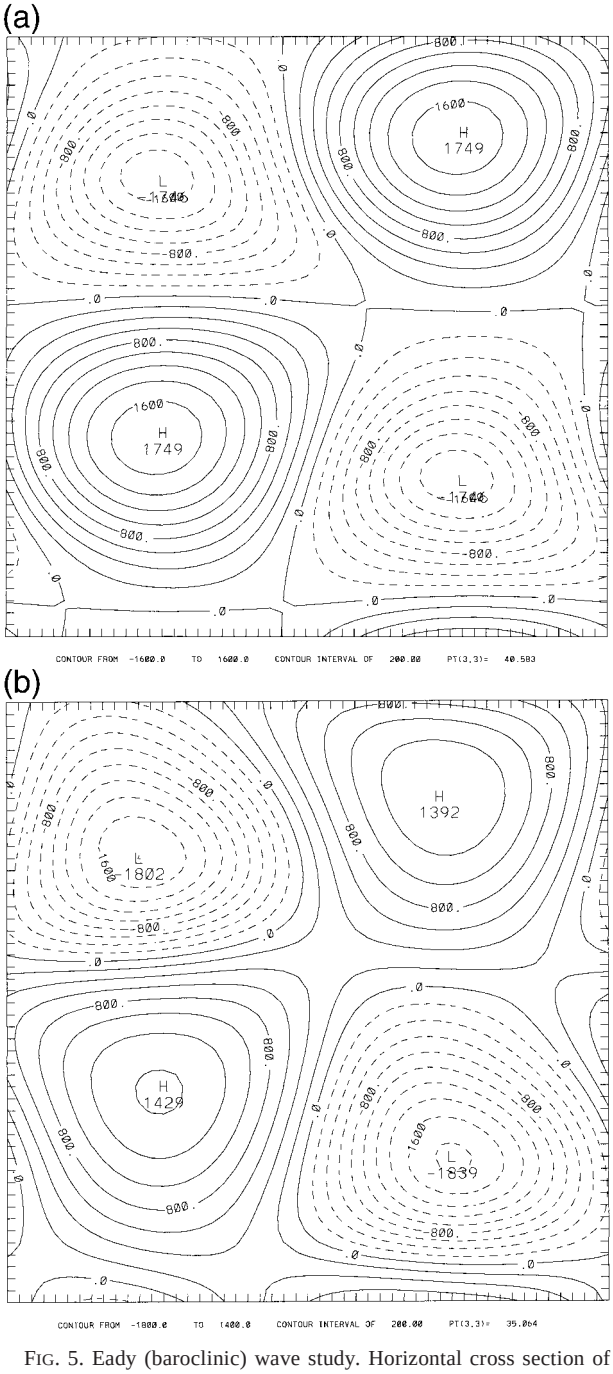

FIG. 5. Eady (baroclinic) wave study. Horizontal cross section of perturbation pressure (Pa) at 9 km. The 120 h S–G solution, shown in (a), is quite similar to the QNH solution, shown in (b).

$$\Phi_{XX} + \Phi_{YY} + \Phi_{ZZ} = 0$$

$$\left(\frac{\partial}{\partial T} + Z\frac{\partial}{\partial X}\right)\Phi_Z - \Phi_X = 0 \quad \text{on } Z = 0,\ 1,$$

where the geostrophic coordinates are defined as $X = x + v_g/f$ and $Y = y - u_g/f$ with u_g and v_g denoting the geostrophic wind on the x and y direction, respectively. The other variables are defined as $Z = z$, $T = t$, $\Phi = \phi + \frac{1}{2}(u_g^2 + v_g^2)$ with ϕ denoting the geopotential.

The above Eady wave problem is a linear second-order homogeneous equation with constant coefficients. The solution to this problem for the most unstable mode at a given λ was shown in Hoskins (1976) as follows:

Unauthenticated | Downloaded 10/04/22 02:19 PM UTC

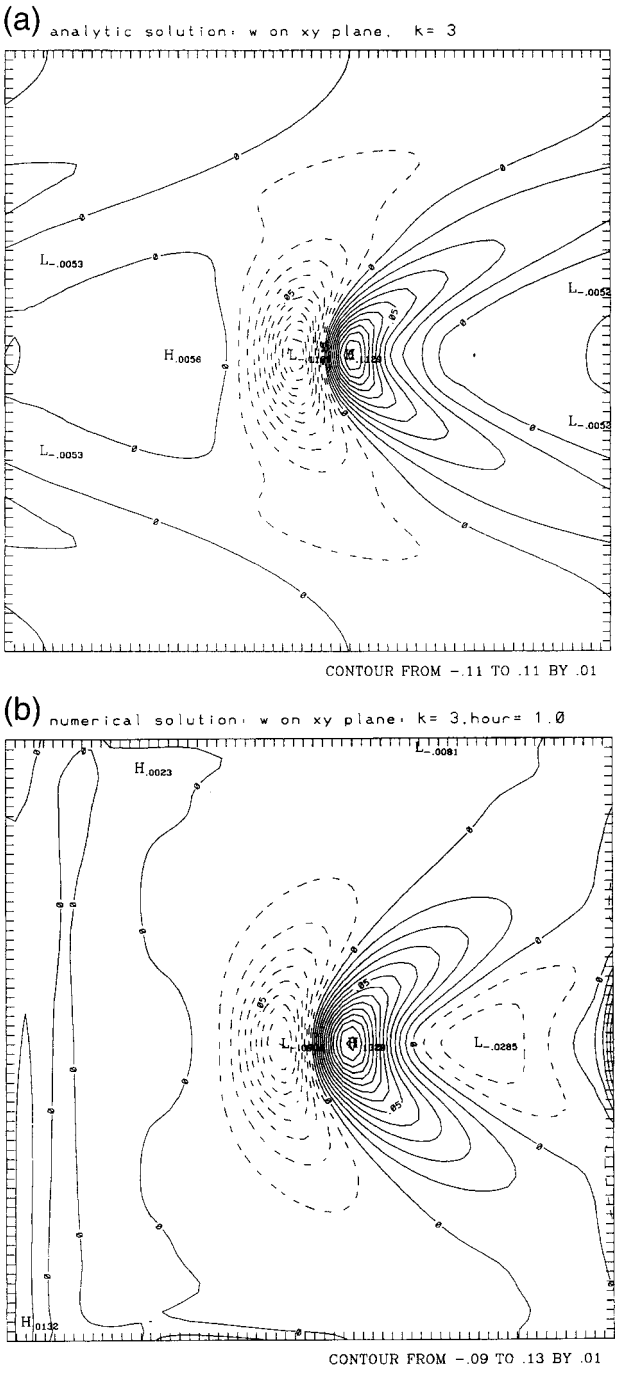

FIG. 6. A comparison of the analytic solution of Smith (1980) for 3D flow over a bell-shaped mountain, with the solution by the fully nonhydrostatic version of QNH. The horizontal size of the domain is 64 km, with the mountain horizontal scale ''a'' equal to 6 km. In (a) the analytic solution for the vertical velocity (m s^{-1}) is plotted on the 3-km horizontal surface, with the 100-m mountain located in the center of the domain. (b) Presents the QNH solution for the same plane.

$$\Phi = e^{\sigma T} \sin\lambda Y(a \sin X' \cosh K_{1,1} Z' + b \cos X' \sinh K_{1,1} Z'),$$

where $X' = X - \frac{1}{2}T$, $Z' = Z - \frac{1}{2}$, $K_{1,1} = (1 + \lambda^2)^{1/2}$, $a/b = [(\gamma \coth\gamma - 1)/(1 - \gamma \tanh\gamma)]^{1/2}$, $\gamma = \frac{1}{2}(1 + \lambda^2)^{1/2}$, and $\sigma \sim 0.3098(1 + \lambda^2)^{-1/2}$.

The most unstable wave for $\lambda = 1$ is used as initial data to derive the baroclinic waves for the S–G solution, as well as for the QNH solution for purpose of comparison. The S–G solution shown in the following includes the higher-order terms to account for the nonlinearity (see Hoskins 1976). The same initial data is used by the QNH model for the simulation of baroclinic waves on the domain size of 5000 km × 5000 km in the horizontal, and 9 km in the vertical. The QNH governing equations used in this simulation are similar to those described in sec. 2a, with no orography (flat lower boundary) and no dissipation. The grid spacing is chosen as 100 km in the horizontal and 1 km in the vertical. Thus the quasi-nonhydrostatic parameter in this run is 10^{-4}. The mean fields used to derive the S–G solution in Hoskins (1976) are also imposed on the QNH model for the simulation of the baroclinic waves. To be consistent with the analytic solution, the lateral boundary conditions for QNH in this simulation are periodic.

The baroclinic waves at the early stage (say before 48 h), for the S–G solution, and the QNH model simulation are very similar. However, as time goes by, the two solutions slowly diverge because the effect of the nonlinearity caused by ageostrophic motions. In the following, we compare the baroclinic waves simulated at the 120th h derived from the S–G solution and the QNH model. The figures are depicted on a vertical cross section along the south–north direction with the low pressure in the south and the high pressure in the north. The left-hand side (lhs) corresponds to south, and the right-hand side (rhs) is north. Figures 4a and 4b are the vertical cross section of the 120-h simulated potential temperature perturbation derived from the S–G solution and the QNH model, respectively. The potential temperatures derived from the S–G solution and the QNH model are similar. The prominent feature in these two figures is the region of large temperature gradients concentrated in the central part of the domain. The temperature lines tilt upward from the south to the north, showing the classical vertical tilt of a front.

Figures 5a and 5b show pressure perturbation fields at the 120th h derived from the S–G solution and the QNH model, respectively. Note that they are displayed on a horizontal plane at 9 km. (The simulated fields in low levels are similar to those in high levels with a reversed sign.) The S–G pressure perturbation shows an antisymmetric pattern. The antisymmetric pattern is due to the symmetry of the S–G solution in the geostrophic coordinates. In contrast, the QNH simulated low pressure system shown in Fig. 5b is more intense than that of the high pressure system. This is consistent with commonly observed frontal pressure systems, which have a deep low center surrounded by a large pressure gradient, while the

Unauthenticated | Downloaded 10/04/22 02:19 PM UTC

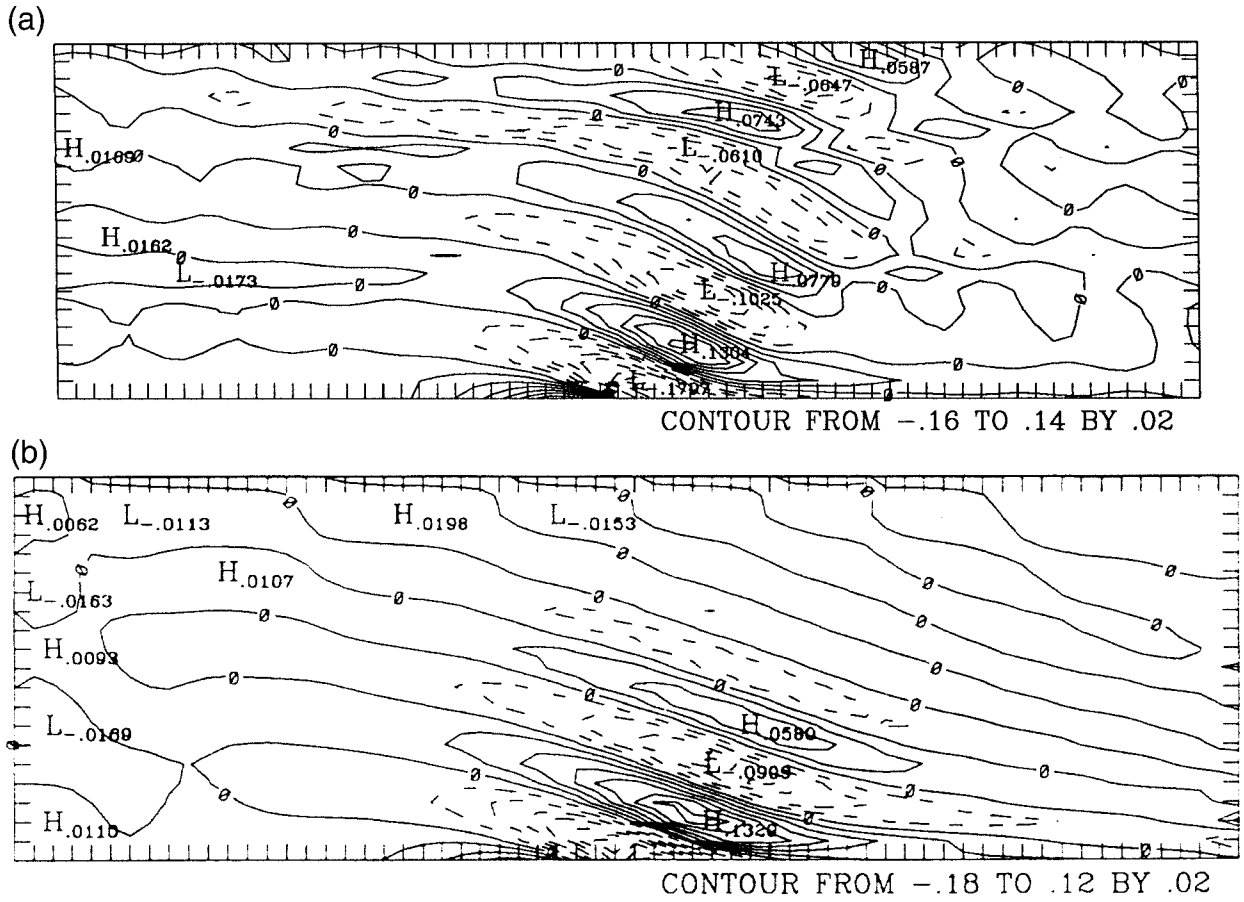

FIG. 7. Similar to Fig. 6 except for a cross section of the Smith (1980) solution and the QNH integration of flow around a bell-shaped mountain. (a) Vertical velocity (m s^{-1}) is presented, with the analytic solution, and (b) the QNH solution.

pressure gradient associated with a high is relatively small. Snyder et al. (1991) found similar differences between the S–G solution and their simulation using a primitive equation. They showed that the systematic differences could be explained in terms of the S–G errors in the ageostrophic vertical vorticity.

In general, the results of the full QNH model were consistent with the S–G analytic solution of Hoskins (1976).

c. Mountain waves

A test was conducted to determine if terrain-forced, vertically propagating gravity waves were properly calculated in the QNH model. To separate this test from the gravity wave effects that are caused by the use of the quasi-nonhydrostatic constant, the mountain wave test was conducted with the fully nonhydrostatic version of QNH. An extensive discussion of the effect of α on mountain waves is given in MacDonald et al. (2000), and also covered in Browning and MacDonald (1993). The test is of the type discussed by Smith (1980), where flow over and around an isolated, bell-shaped mountain is solved in three dimensions by linearization. Following Smith, we used a bell-shaped mountain with circular topography where ''h'' and ''a'' are the mountain height and horizontal scale. We used a height of 100 m, and a horizontal scale of 6 km. Note that at this scale the theory indicates a fully nonhydrostatic model should be used. The mountain was centered in a domain of 64 km by 64 km, with the top of the model located at 20 km. Stability is constant with height. The horizontal and vertical mesh lengths of the model were 1 km; as discussed in MacDonald et al. (2000), a fully nonhydrostatic model is most efficient if it has its vertical and horizontal grid distances equal. As was done by Smith, the ''analytic'' steady-state solution is obtained by using linear theory for a hydrostatic, Boussinesq fluid. The small amplitude of the mountain and the flow make the results relevant for the nonhydrostatic, nonlinear case. It is solved using superposition of Fourier components for the bottom boundary.

The mountain wave test was initialized in a motionless state, with the flow increasing from 0 to 10 m s^{-1} during the first 30 min. The QNH model was integrated in time for several hours. It established a pattern that began to resemble the analytic solution within the first hour. Figure

Unauthenticated | Downloaded 10/04/22 02:19 PM UTC

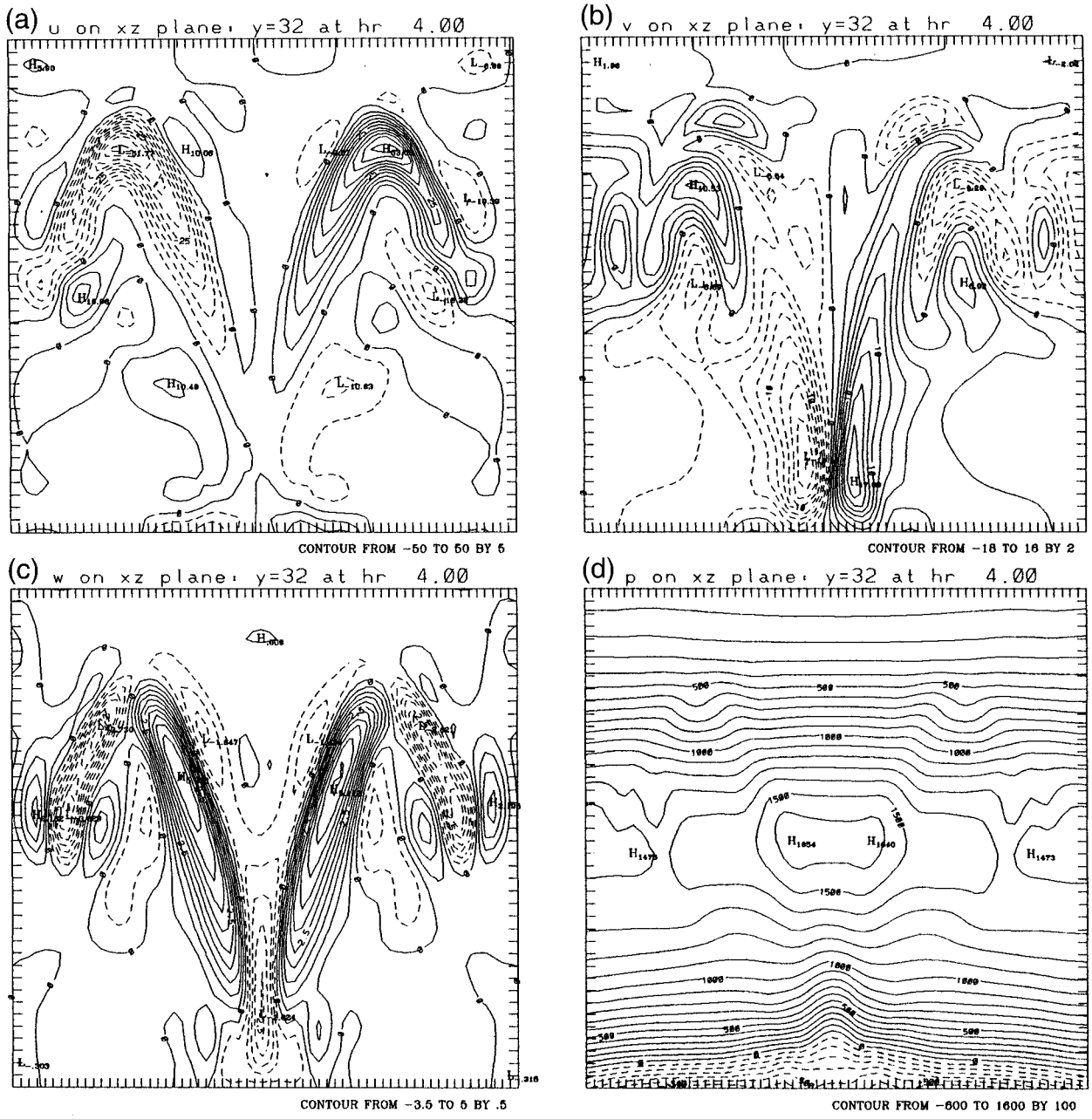

FIG. 8. Four cross sections through a simulated tropical storm after 4 h of heating in a Gaussian annulus of 30-km radius. The heating is centered at 5 km in the vertical, and is also Gaussian in time. (a) The west wind (u) on an east–west cross section in m s^{-1}. It can be interpreted as the divergent component of wind. (b) The north–south (v) component of the wind (m s^{-1}), which can be interpreted as the radial flow. (c) The vertical velocity, w. (d) The perturbation pressure (Pa).

6a shows the analytic solution for vertical velocity (m s^{-1}) at 3 km altitude), with the QNH solution after a 1 h integration shown in Fig. 6b. The two patterns closely resemble each other. Note that the downward motion over the mountain is about 9 cm s^{-1} in the model, but 11 cm s^{-1} in the analytic solution. This difference may by due to the nonhydrostatic effects of wave propagation directly above the mountain in the model. The first downstream upward motion area is 13.3 cm s^{-1} in the model, and 12.9 cm s^{-1} in the analytic solution. Figure 7a shows a cross section of the analytic solution for the vertical velocity (m s^{-1}) centered on the mountain. The model solution is shown in Fig. 7b. The fields resemble each other. The characteristic look of vertically propagating gravity waves being carried downstream by the westerly flow is evident. One difference notable in Fig. 7 is that the analytic solution continues the wave train up into the stratosphere, while the model damps the wave train at the tropopause. The

Unauthenticated | Downloaded 10/04/22 02:19 PM UTC

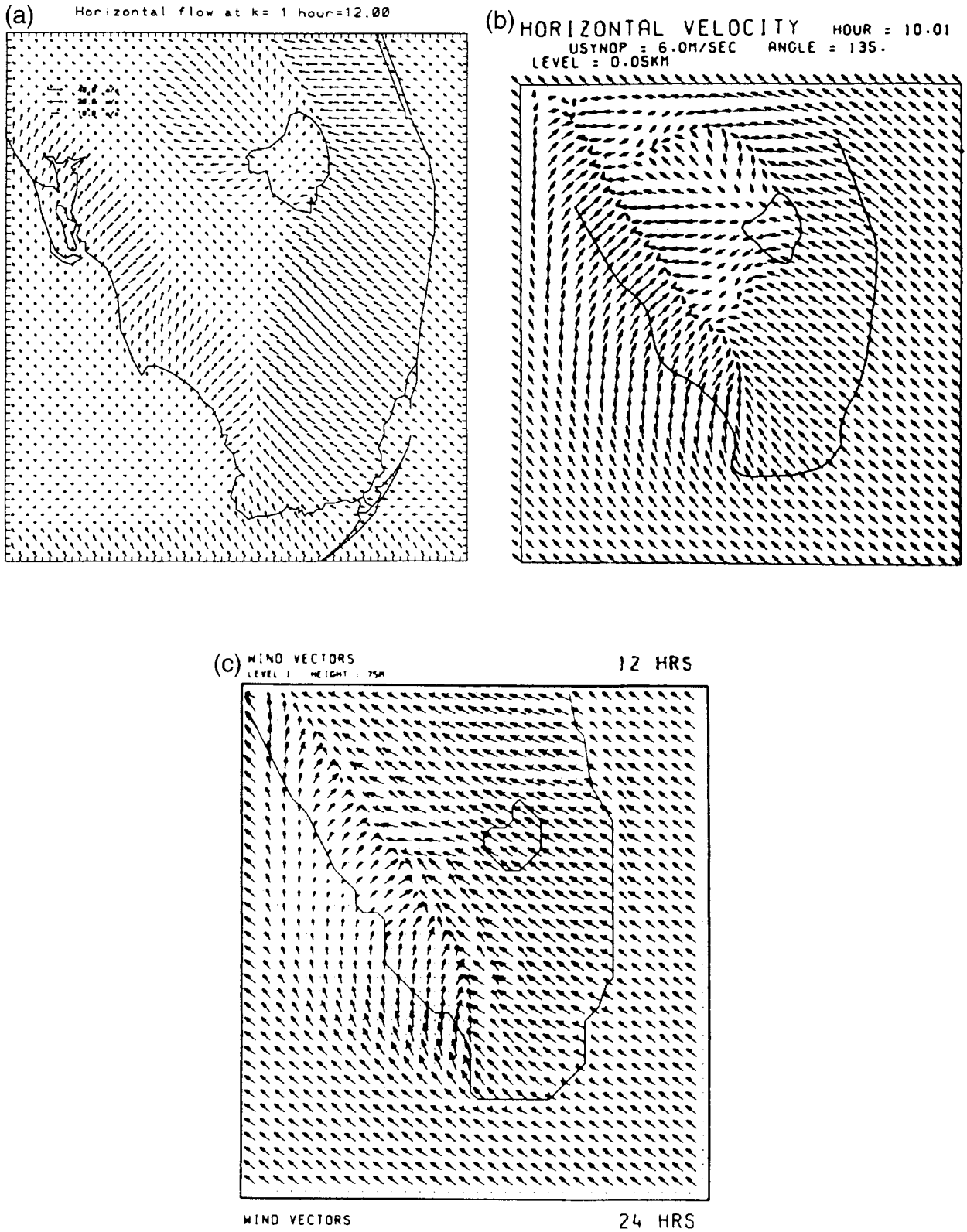

FIG. 9. Sea-breeze simulation for southern Florida. Winds are shown as vectors, with length of vector proportional to velocity. (a) The result of the QNH 12-h prediction is shown. (b) The results of Pielke's (1974) simulation are shown at 10 h. (c) The result of a 12-h simulation by Tapp and White's (1976) nonhydrostatic model is shown.

Unauthenticated | Downloaded 10/04/22 02:19 PM UTC

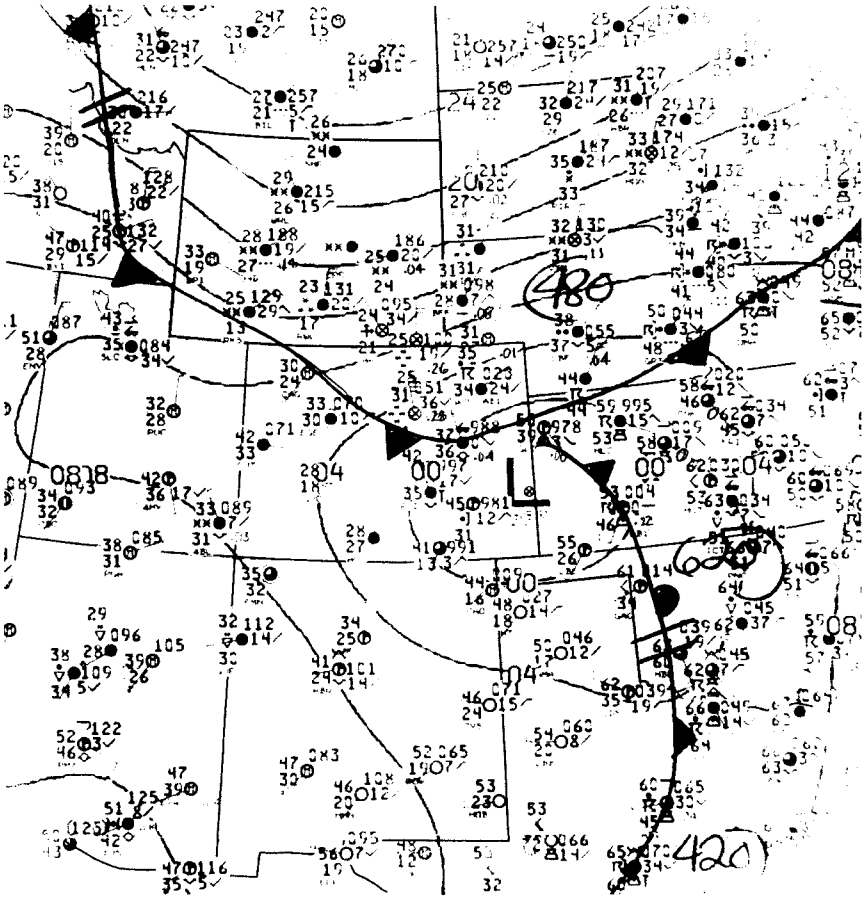

FIG. 10. Surface analysis from NMC for the Colorado area at 0300 UTC 9 March 1992.

analytic solution does not include the rapid change in stratification at the tropopause, so it is not valid to compare above that level.

The conclusion of the mountain wave test is that the proper linear, hydrostatic solution for vertically propagating waves is obtained in the nonhydrostatic version of the QNH model.

d. Tropical storm

The tropical storm simulation was done by letting a Gaussian annulus of heating 30 km in radius grow smoothly in time, from 0 to 4 J kg^{-1} over a period of 6 h. After 6 h, the heating was kept constant. The pattern of heating was Gaussian in the vertical, and centered at 5 km in a vertical domain of 20 km. The use of the Gaussian functions in three dimensions is to attain the required smoothness needed in a quasi-nonhydrostatic model. The storm was centered in a horizontal domain of 640 km $\times$ 640 km. The model used a quasi-nonhydrostatic constant $\alpha = 10^{-2}$, with a horizontal resolution of 10 km. The initial state of the model was based on the sounding from Palm Beach, Florida, at 0000 UTC 24 August 1992, right before landfall of Hurricane Andrew in southern Florida. Sea surface temperature was taken as 30°C. The heating generated vertical motion, which resulted in precipitation, and a dynamic system, which had many similarities to the eyewall and environs of a tropical storm. The low-level circulation of the system reached 20 m s^{-1} at about 5 h, and reached 40 m s^{-1} at about 10 h.

The tropical storm test was designed to test a number of the weather prediction aspects of the full-physics QNH model. It was the first test to fully illustrate the value of the well-posed lateral boundary, and also to test the vertical (top) boundary. It thoroughly exercised the microphysical part of the model physics, as well as the Mellor–Yamada (1974) turbulence scheme. Radiation and surface forcing were also tested.

Figure 8 shows four cross sections through the center of the storm at 4 h. On the upper left, Fig. 8a, the u component of the wind is shown for an x–z plane, which can be interpreted as the divergent component of the wind. Notice the very strong outflow at high levels in the strongly forced situation. At low levels, the convergence is strong immediately outside and under the eyewall. Figure 8b shows the v component of the wind, which for the x–z cross section is the rotational component of flow. At four hours the circulation has reached a maximum of 18 m s^{-1}

Unauthenticated | Downloaded 10/04/22 02:19 PM UTC

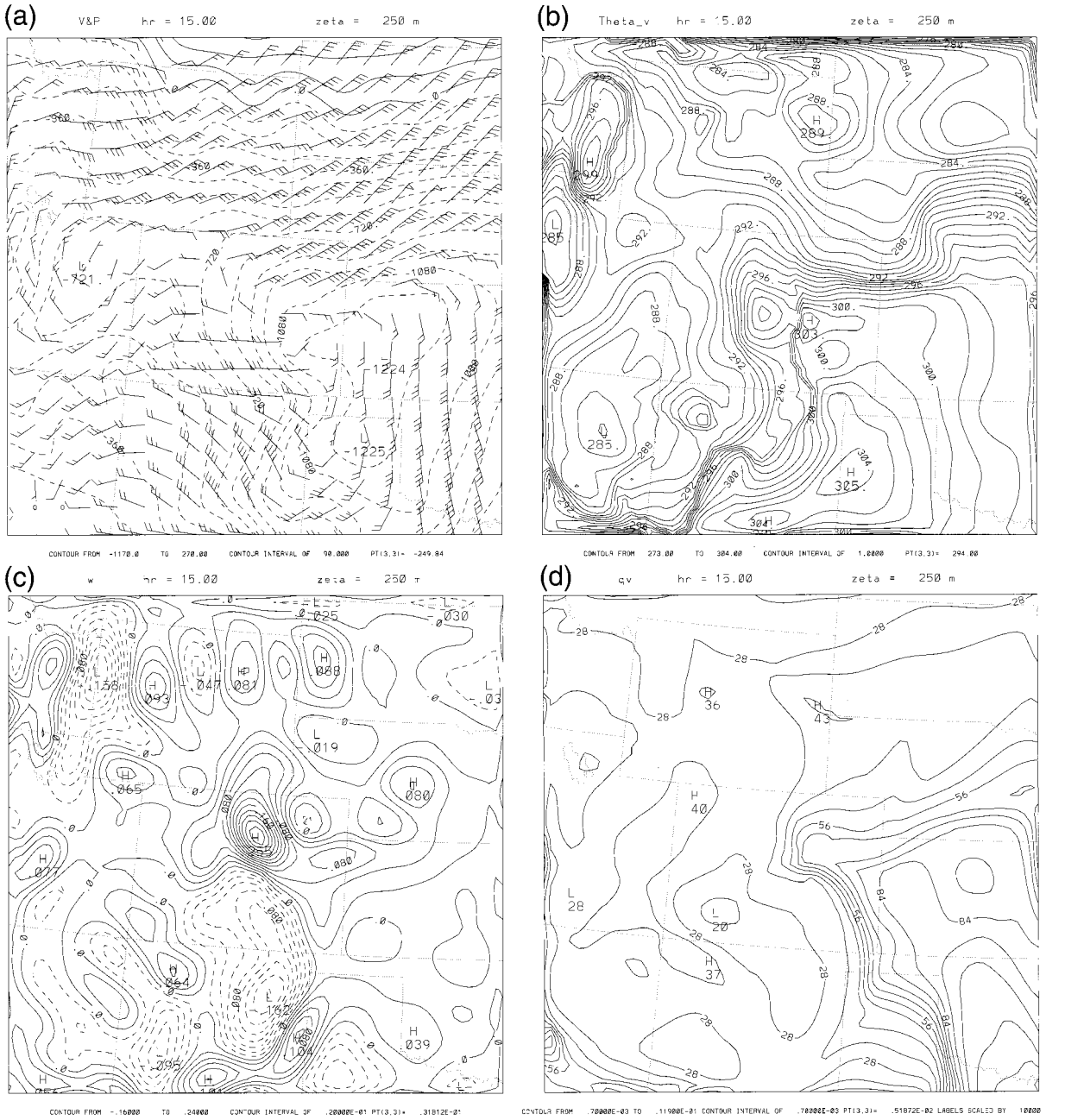

FIG. 11. QNH model simulation after 15 h of integration, valid at 0300 UTC 9 March 1992. (a) Wind barbs (kt) show strong northeasterly flow behind the front in northern Colorado. The perturbation pressure analysis (Pa) shown by dashed lines, has a low on the Colorado–Kansas border, with troughs extending northeast and northwest from the center. (b) Same as (a) except it presents potential temperature. (c) Same as (a) except it presents vertical velocity (m s^{-1}) at the 250 m surface. (d) Same as (a) except it presents the specific humidity in g $kg^{-1} \times 10$.

centered at 2 km above the surface. The vertical velocity, shown in Fig. 8c, has a maximum upward value of 5 m s^{-1}, in the eyewall, and a sinking zone of 2 m s^{-1} in the center of the eye. The perturbation pressure shown in Fig. 8d with units of pascals, shows a warm core low at low levels, and a strong anticyclone centered over the storm near the tropopause. Observational studies of tropical storms such as that of Jorgenson (1985) show that the structure obtained rather simply by a heating annulus in QNH is quite reasonable.

e. Sea breeze

Although this study is titled ''sea breeze'' after the pioneering work of Pielke (1974), it is really a mesoscale study of the low-level flow over a 300-km pen-

Unauthenticated | Downloaded 10/04/22 02:19 PM UTC

insula surrounded by tropical ocean. In our study we ran a QNH2 model for 24 h with both wet and dry conditions. The run was compared with the hydrostatic model simulation of Pielke (1974) and the nonhydrostatic model run of the same situation done by Tapp and White (1976). The primary purpose of this effort was to test the radiation, surface forcing, and boundary layer packages of the model. Following Pielke, we initialized the model in the early morning, and used the same large-scale variables and parameters. In particular, we used the potential temperature and moisture soundings, and the horizontal wind as specified on p. 122 of Pielke's article. We also used a similar horizontal grid spacing of 10 km, although QNH2 vertical spacing of 1 km is more coarse in the boundary layer.

The result of the model integrations were similar to the results obtained by Pielke's hydrostatic model, and by Tapp and White's nonhydrostatic model. The results of the three models for surface flow over Florida are shown in Fig. 9. The QNH prediction for 12 h is shown in (a), Pielke's prediction for 10 h is shown in (b), and Tapp and White's 12-h prediction is shown in (c). Their are some differences among the three. In QNH, southeast wind pushes the east coast sea breeze front well inland, while the west coast front is held within 50 km of the ocean. In all three models Lake Okeechobee establishes a mesoscale outflow as the differential solar heating over the lake interacts with the surrounding land. This effect is quite strong in Pielke's simulation, nearly as strong in QNH and significantly weaker in Tapp and White.

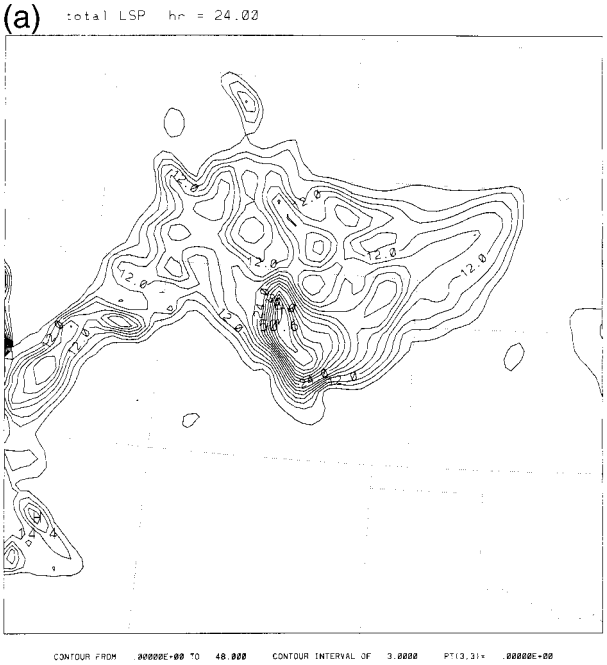

FIG. 12a. Precipitation (mm) over the 24-h period from 1200 UTC 8 March 1992 to 1200 UTC 9 March. A maximum of 50.6 mm was simulated over Colorado's Front Range, with a lobe of heavier precipitation extending down to the Palmer Ridge (south of Denver) and northeastward toward the northeastern corner of the state.

f. Winter storm

The last and most complete test of the QNH model was a winter storm, which hit Colorado's front range on the evening of 8 March 1992. The storm was particularly strong, with over 20 in. of snow during a 12-h period, lightning, and winds over 50 kt. It was felt that such a storm would be a good test of the mesoscale prediction capabilities of the model. The fact that the storm was very wet, developed over steep mountain terrain, and was strongly baroclinic exercised several important aspects of the model. We have referred to this as a simulation. It is well known that use of actual diagnosed lateral boundary conditions make a prediction better by reducing one source of inaccuracy. In this case the purpose was to determine if the model was operating properly, so the elimination of one source of uncertainty helped to attain this goal. The model run was based on real data for its initialization, but it used boundary conditions from the MAPS (Bleck and Benjamin 1993) model diagnosis at 3-h intervals. In this paper we will give a short summary of the relevant test results, specifically, that the basic fields of wind, temperature, and moisture were well predicted over a 24-h period, and that the model-simulated precipitation was quite accurate. A more complete discussion of the test and its results is presented in Lee and MacDonald (2000).

In the winter storm test a QNH3 model was run, with horizontal resolution of 20 km, vertical resolution of 500 m, and a quasi-nonhydrostatic parameter of $\alpha = 0.000\,625$. Instead of the Mellor–Yamada turbulence scheme, we used the drag formulation for the boundary layer discussed in section 2.6, because it gave a better result. The model was initialized using the bounded-derivative technique at 1200 UTC 8 March 1992, and run for 24 h.

This discussion will be limited to one prediction time, 0300 UTC 9 March. The surface chart from the National Meteorological Center [NMC, now known as the National Centers for Environmental Prediction (NCEP)] is presented in Fig. 10. A cold front has pushed into the central part of eastern Colorado, with heavy snow being reported at front-range weather stations. The weather map also shows very moist air, with dewpoints in the 50s, ahead of a north–south-oriented front in Kansas. Strong north to northeasterly winds are seen in northern Colorado, western Nebraska, and southeastern Wyoming. Figure 11 presents the QNH prediction for the same time, 0300 UTC 9 March, which is 15 h after initialization. These results can be compared with the Regional Atmospheric Modeling System (RAMS) model runs discussed by Snook (1994). The chart on the upper left, Fig. 11a, has the winds in knots and the pressure perturbation (Pa) at 250 m above the ground.

Unauthenticated | Downloaded 10/04/22 02:19 PM UTC

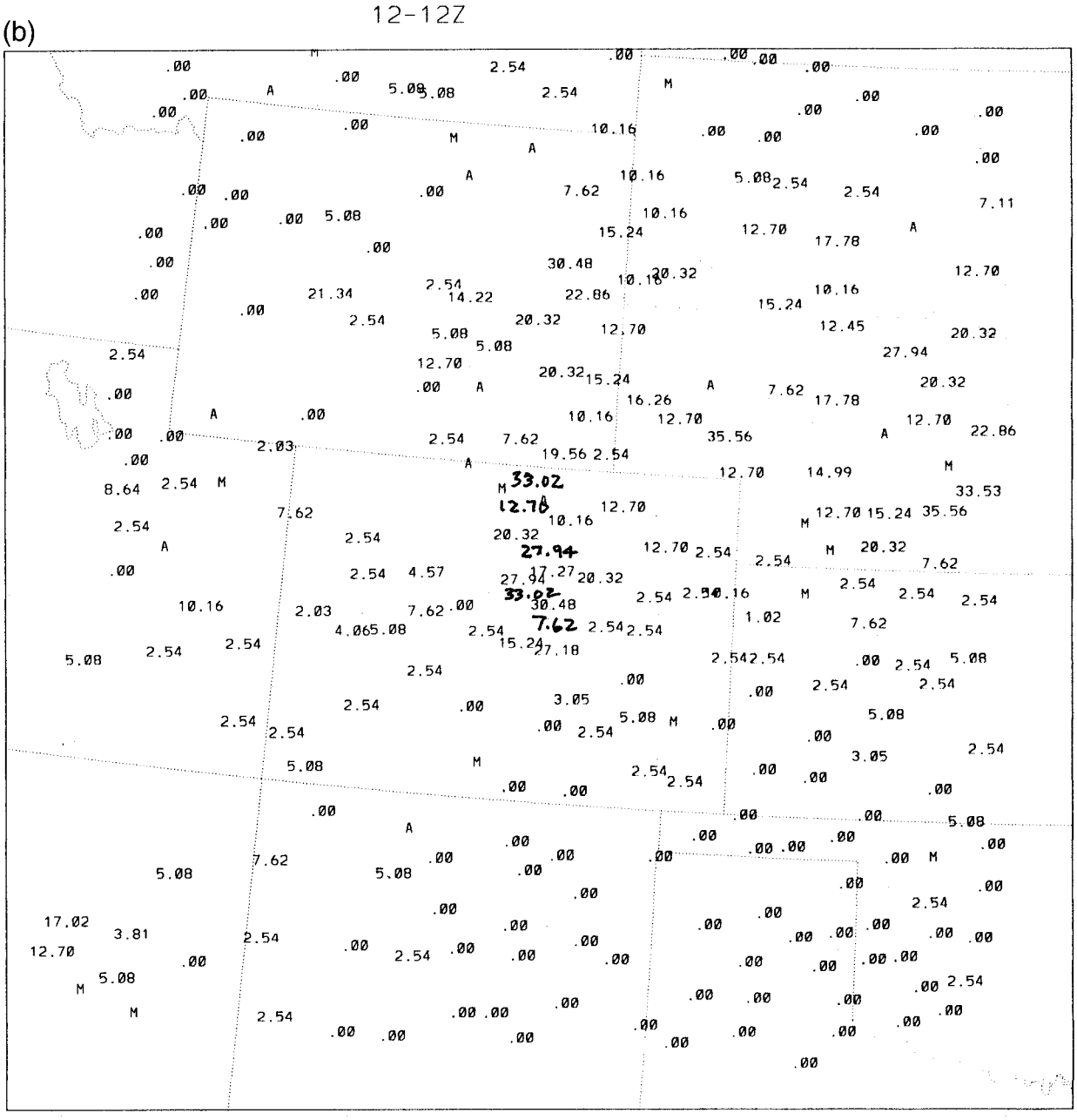

FIG. 12b. Measured precipitation (mm) for same period as (a).

Note the strong northeast winds in northeast Colorado, western Nebraska, and southeast Wyoming. Figure 11b presents the model-predicted virtual temperature (K). Note the well-defined, strong front in central Colorado. Figure 11c presents the vertical velocity (m s^{-1}) at 250 m, which at this level is primarily due to terrain forcing. Most noteworthy is the center of 32 cm s^{-1} of rising motion over the front-range. A crossection of the vertical motion field is given in Lee and MacDonald (2000). Figure 11d shows the water vapor specific humidity (grams $kg^{-1} \times 10$). This shows that the plume of very moist air in Kansas was swept into the circulation along the front, and was contributing to the very heavy snow seen on the surface weather map (Fig. 10).

Figure 12a shows the 24-h precipitation prediction from the QNH model, with a plot of the observed precipitation shown in Fig. 12b. The QNH simulation shows a strong maximum in the foothills of the Rockies, west of the Front Range, of 50.6 mm of precipitation. This maximum curls around and extends northeastward

Unauthenticated | Downloaded 10/04/22 02:19 PM UTC

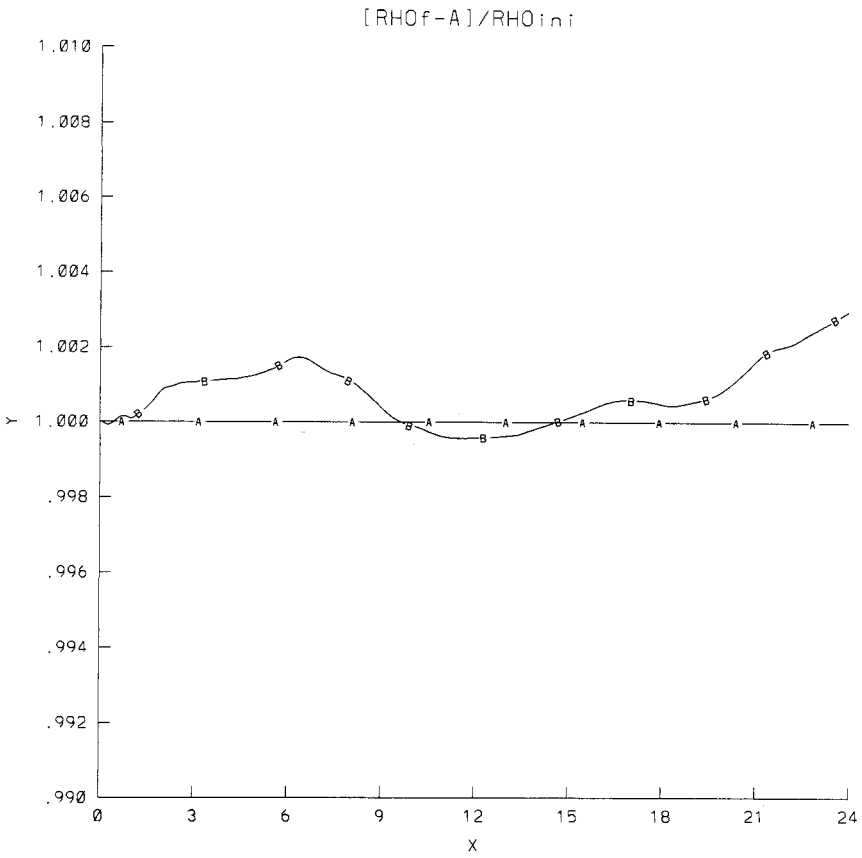

FIG. 13. Conservation of mass in the model for the winter storm case. The line A-A-A represents perfect conservation, while the line B-B-B shows what happened during the model integration. The mass is generally conserved within about one-third of a percent.

into Nebraska, approximately aligned with the strongly dynamic situation during the period from 0000 to 0600 UTC 9 March. The RAMS prediction described by Snook (1994) for the period from 2100 UTC 8 March to 0900 UTC 9 March showed a similar pattern, with a lobe of 20–40 mm of precipitation along the east side of the continental divide, a maximum in excess of 60 mm south of Pikes Peak, and another lobe of precipitation along the central ridge of eastern Colorado (i.e., the Palmer ridge). In contrast, the NMC's Nested Grid Model showed only about 9 mm of precipitation during the period from 0000 to 1200 UTC 9 March. We ran the winter storm case with the Kuo (1974) cumulus paramaterization included. It had very little effect, with a maximum of sub-grid-scale precipitation of less than 10 mm.

The main differences between model types can be learned from the results presented by Snook (1994) and those presented in this paper. The lower resolution hydrostatic models had much lower amounts of precipitation, as should be expected for a strong mesoscale event of this type. The nonhydrostatic model, RAMS, produced similar precipitation amounts, but appeared to be more noisy. The difference in precipitation skill due to the difference in accuracy of the two models cannot be determined from a single case.

4. Conclusions

a. Model evaluation criteria

This paper reports on the design and testing of a new mesoscale weather prediction model. Pielke (1984) has identified evaluation criteria that a mesoscale model should meet before the credibility of the simulations can be established by the scientific community. In this section, the six criteria are listed, along with the listing of how the QNH model development has addressed the criteria:

1) MODEL COMPARED WITH KNOWN ANALYTIC SOLUTIONS

The model was compared with four known analytic solutions. In MacDonald et al. (2000), it was compared with Long's solution for terrain-forced gravity waves. The second was the barotropic, circular vortex discussed in section 3a. The third was the Eady wave described

Unauthenticated | Downloaded 10/04/22 02:19 PM UTC

in section 3b, which showed that the model develops a proper solution for a baroclinic and nonlinear weather situation. The fourth solution was the three-dimensional mountain wave solution developed by Smith (1980) and presented in section 3c.

2) Nonlinear simulations must be compared with other models

The model was compared with other models in three cases. The first was the Florida sea breeze case, presented in sec. 3e, which was first done by Pielke (1974), and since done by many models. The second was the tropical storm, presented in section 3d, which may be compared with other simulations such as Kurihara and Bender (1982). The third is the winter storm of 8 and 9 March 1992, presented in section 3f, which has been simulated by the RAMS, Nested Grid Model (NGM), and MAPS models (Snook 1994).

3) Mass and energy conservation

The mass and energy budgets were calculated for the winter storm case (and other cases). The result of the mass budget calculation is presented in Fig. 13. The total of a conserved quantity (e.g., mass, energy, or water mass) should be the initial mass, as modified by the flux of mass through the boundaries. In Fig. 13, it can be seen that perfect conservation of mass would result in a constant value of 1.00, as represented by line A-A-A. The model varied slightly from perfect conservation, as seen on line B-B-B, with a maximum variation at the end of the period of less than ⅓%. A similar calculation was done for energy. The energy varies slowly, with the maximum error at the end of the period of about ½%. Since the model includes water mass, we have also calculated the water mass budget. In this case, precipitation is treated as a loss of mass through the bottom boundary. The error reached a maximum of ¾% at 18 h and then decreased. In summary, the model conserved mass, energy, and water mass reasonably well.

4) Model predictions quantitatively compared with observations

The only actual prediction (simulation) done so far by the QNH model is the winter storm case. As discussed in section 3f, the model did well on all fields, particularly precipitation. As discussed below, the next step is to test the model predictions in a large number of cases.

5) Computer logic of the model must be available on request

The model is in the public domain. The source code is available on the World Wide Web at http://fsl.noaa.gov/qnh/user.guide.

6) Published model subjected to peer review

This is addressed by the current paper.

b. Summary

The main purpose of the effort described in this paper was to determine if quasi-nonhydrostatic models in general, and the QNH model in particular, could be valuable in mesoscale prediction. The development of a full physics mesoscale weather prediction model allowed a test of a theory of modeling that has been extensively studied (Browning and Kreiss 1986), but has had limited use for real prediction. The results of the test program suggest that quasi-nonhydrostatic models may be useful for weather prediction, particularly of cloud and precipitation. Furthermore, the theoretical advantages of well-posed models seemed to be evident in the results. Specifically, the prediction of the tropical storm and the winter storm showed realistic results for mesoscale structures. It is thought that this is a result of the well-posed nature of quasi-nonhydrostatic models. It was also evident in the test program that the well-posed boundaries confer a number of advantages, such as amenability to nesting.

c. Future role of QNH

We see a potential role for the model in regional-scale modeling (domains of approximately 20 million square kilometers, or about double the size of the 48 contiguous United States) at horizontal grid lengths between 20 km and 2 km. A number of models are being tested and developed at these scales; however, the smallest operational model grid mesh in use is the NCEP Meso-Eta model, which is being run at approximately 30-km resolution. The period in which operational mesoscale models will have horizontal resolutions between 20 km and 2 km is approximately the 20-yr period between the year 2000 and 2020. This is partly based on the operational model history, which has taken about 20 yr to go from resolutions between 200 km and 300 km (the Limited Fine Mesh model of the 1970s) to todays resolution of the Meso-Eta, approximately an order of magnitude less in the horizontal. It can also be arrived at by noting the historical increase in the rate of the fastest supercomputers, which has steadily increased at a rate of about 40% per year from the 1950s to the 1990s. If a model increases in processing requirements by a factor of 10 each time the resolution is halved, then a 2.5-km model requires 1000 times the processing power needed for a 20-km model. At an increase of 40% yr^{-1} it takes 20.5 yr to increase computing speed by a factor of 1000.

Quasi-nonhydrostatic models may be valuable for very short-range prediction. The use of the bounded derivative initialization allows a smooth start, even in the presence of topographic forcing or heating. This would allow use of satellite, radar, and surface obser-

Unauthenticated | Downloaded 10/04/22 02:19 PM UTC

vations to obtain latent heating as a function of space, and have the model dynamically adjusted and thus useful for prediction within the first hour. Models of 3-, 6-, or 12-h duration could be initialized and used on schedules that match their usage. Aviation, for example, could use mesobeta-scale models that run frequently for short timescales, and ''keep up'' with the weather as seen by mesoscale observing systems such as satellite and radar. Also, the smoothness of the well-posed boundaries make the use of small domains more feasible.

The use of a well-posed model for variational analysis may be important. The characteristic of accommodating slow mode Rossby scales, but eliminating small high-frequency gravity waves, may help the convergence of four-dimensional variational analysis integrations. If a transient gravity wave is too small to be predicted with proper phase, it is better not to have the wave in the model integration, where it will not in general be matched by observations with gravity wave phase information.

As a result of the test program presented in this paper, it is concluded that the QNH model may be valuable for mesoscale weather prediction.

Acknowledgments. This paper is dedicated to Clive Baillie, who along with his wife Julie, died in a mountain climbing accident on 12 October 1996. Clive knew computers like Stradivari knew violins; he made QNH play right.

REFERENCES

Arakawa, A., and V. R. Lamb, 1977: Compatible design of the basic dynamical processes of the UCLA general circulation model. *Methods in Compatible Physics,* Vol. 17, Academic Press, 174–265.

Baillie, C. F., A. E. MacDonald, J. L. Lee, and S. Sun, 1995: QNH: A portable, parallel, multiscale quasi-nonhydrostatic meteorological model. *Applications of High Performance Computing in Engineering IV,* H. Power, Ed., Computational Mechanics Publications, 1995–2202.

——, ——, and ——, 1996: QNH: A numerical weather prediction model developed for Massively Parallel Processors. *EUROSIM 96,* Elsevier Science B. V., 399–504.

Bleck, R., and S. G. Benjamin, 1993: Regional weather prediction with a model combining terrain-following and isentropic coordinates. Part I: Model description. *Mon. Wea. Rev.,* **121,** 1770–1785.

Browning, G. L., and H.-O. Kreiss, 1986: Scaling and computation of smooth atmospheric motions. *Tellus,* **38A,** 295–313.

——, and A. E. MacDonald, 1993: Incorporating topography into the multiscale systems for the atmosphere and oceans. *Dyn. Atmos. Oceans,* **18,** 119–149.

——, and H.-O. Kreiss, 1994: Splitting methods for problems of different time scales. *Mon. Wea. Rev.,* **122,** 2614–2622.

Dudhia, J., 1993: A non-hydrostatic version of the Penn State/NCAR Mesoscale Model: Validation tests and simulation of an Atlantic cyclone cold front. *Mon. Wea. Rev.,* **121,** 1493–1513.

Durran, D. R., 1991: The third-order Adams–Bashforth method: An attractive alternative to leapfrog time differencing. *Mon. Wea. Rev.,* **119,** 702–720.

Gal-Chen, T., and R. C. Somerville, 1975: On the use of a coordinate transform for the solution of the Navier–Stokes equations. *J. Comput. Phys.,* **17,** 209–228.

Grell, G. A., J. Dudhia, and D. R. Stauffer, 1994: A description of the fifth-generation Penn State/NCAR Mesoscale Model (MM5). NCAR Tech. Note, NCAR.TN-398+STR, 122 pp. [Available from NCAR Publications, P.O. Box 3000, Boulder, CO 80307.]

Gustafsson, B., H.-O. Kreiss, and J. Oliger, 1995: *Time Dependent Problems and Difference Methods.* John Wiley and Sons, 642 pp.

Haltiner, G. J., and R. T. Williams, 1980: *Numerical Prediction and Dynamic Meteorology.* John Wiley and Sons, 477 pp.

Hoskins, B. J., 1976: Baroclinic waves and frontogenesis. Part I: Introduction and eady waves. *Quart. J. Roy. Meteor. Soc.,* **102,** 103–122.

Jorgenson, D., 1985: Vertical motions in intense hurricanes. *J. Atmos. Sci.,* **42,** 840–856.

Kreiss, H.-O., 1980: Problems with different time scales for partial differential equations. *Comm. Pure Appl. Math.,* **33,** 399–440.

Kuo, J., 1974: Further studies of the parameterization of the influence of cumulus convection on large-scale flow. *J. Atmos. Sci.,* **31,** 1232–1240.

Kurihara, Y., and M. A. Bender, 1982: Structure and analysis of the eye of a numerically simulated tropical cyclone. *J. Meteor. Soc. Japan,* **60,** 381–395.

Lee, J. L., and A. E. MacDonald, 2000: QNH: Mesoscale bounded derivative initialization and winter storm test over complex terrain. *Mon. Wea. Rev.,* **128,** 1037–1051.

MacDonald, A. E., J. L. Lee, and Y. Xie, 2000: On the use of quasi-nonhydrostatic models for mesoscale weather prediction. *J. Atmos. Sci.,* **128,** 1037–1051.

Mellor, G. L., and T. Yamada, 1974: A hierarchy of turbulence closure models for planetary boundary layers. *J. Atmos. Sci.,* **31,** 1791–1806.

Oliger, J., and A. Sundstrom, 1978: Theoretical and practical aspects of some initial boundary value problems in fluid dynamics. *SIAM J. Appl. Math.,* **35,** 419–446.

Orlanski, I., 1975: A rational subdivision of scales for atmospheric processes. *Bull. Amer. Meteor. Soc.,* **56,** 527–530.

Pielke, R. A., 1974: A three-dimensional numerical model of the sea breezes over South Florida. *Mon. Wea. Rev.,* **102,** 115–139.

——, 1984: *Mesoscale Meteorological Modeling.* Academic Press, 612 pp.

Schultz, P., 1995: An explicit cloud physics parameterization for operational numerical weather prediction. *Mon. Wea. Rev.,* **123,** 3331–3343.

Skamarock, W. C., and J. B. Klemp, 1994: Efficiency and accuracy of the Klemp–Wilhelmson time-splitting technique. *Mon. Wea. Rev.,* **122,** 2623–2630.

Smith, R. B., 1980: Linear theory of stratified hydrostatic flow past an isolated mountain. *Tellus,* **32,** 348–364.

Snook, J. S., 1994: An investigation of Colorado Front Range winter storms using a nonhydrostatic mesoscale numerical model designed for operational use. NOAA Tech. Memo. ERL FSL-10, 373 pp. [Available from Forecast Systems Laboratory, Boulder, CO 80303.]

Snyder, C., W. C. Skamarock, and R. Rotunno, 1991: A comparison of primitive-equation and semigeostrophic simulations of baroclinic waves. *J. Atmos. Sci.,* **48,** 2179–2194.

Stephens, G. L., 1978: Radiation profiles in extended water clouds. Part II: Parameterization schemes. *J. Atmos. Sci.,* **35,** 2111–2122.

Tao, W.-K., and J. Simpson, 1993: Goddard Cumulus Ensemble Model. Part I: Model description. *Terr., Atmos. Oceanic Sci.,* **4,** 35–72.

Tapp, M. C., and P. W. White, 1976: A nonhydrostatic mesoscale model. *Quart. J. Roy. Meteor. Soc.,* **102,** 277–296.

Washington, W. M., and C. L. Parkinson, 1986: *An Introduction to Three-Dimensional Climate Modeling.* University Science Books, 422 pp.

Unauthenticated | Downloaded 10/04/22 02:19 PM UTC